

Satellite observation highlights of the 2010 Russian Wildfires

Jacquelyn C. Witte¹, Anne R. Douglass², Bryan N. Duncan², Arlindo da Silva², and Omar Torres²

¹Science Systems and Applications Inc. Lanham, MD, 20703, USA

²NASA Goddard Space Flight Center, Code 613.3, Greenbelt, MD 20771, USA

From mid-June 2010 through August western Russia experienced an unprecedented heat wave characterized by prolonged high temperatures (~ 40degC) and drought conditions. The heat wave set-up the ideal meteorological conditions for an unprecedented wildfire event. Plumes of thick smoke and burning pollution products were reported over highly populated regions including the capitol city of Moscow. The negative human and economic impacts were severe and extensively covered by the local and international media.

Our study took advantage of the large complement of NASA's Earth Observing System (EOS) sensors to track and quantify the source of the thick smoke and wildfire byproducts, such as carbon monoxide (CO), which settled over Moscow and nearby cities. A typical tracer of carbonaceous (or smoke) aerosols produced from wildfires smoke aerosols is the Aerosol Index (AI) that is measured by the Ozone Monitoring Instrument (OMI) on-board the Aura satellite. Over Moscow, OMI measured unprecedented levels of smoke aerosols between the end of July and mid-August that were an order of magnitude higher than previous summers going back to the earliest record in 2005. Likewise, CO, measured by the Atmospheric Infrared Sounder (AIRS) on-board Aqua, showed exceptionally high levels over Moscow. Previous summers going back to 2003 typically have an average CO concentration of 20×10^{17} molecules/cm². However, during the peak of the 2010 wildfires, CO averaged around 35×10^{17} molecules/cm². To put this wildfire event into perspective, the magnitude of the CO we observed over Moscow was equivalent to the 2006 El Nino wildfire event over Indonesia where some of the most intense wildfires have been documented.

Using the MODIS fire count data on-board the Aqua and Terra satellites, we observed numerous wildfires throughout western Russia and Eastern Europe that raged for almost three weeks between the end of July and mid-August. During this time period air-parcel back-trajectories initiated from Moscow traced the origin of the enhanced smoke pollution from wildfires raging in the southeast. The MODIS Fire Radiative Power (FRP) product measured very intense of the fires clustered in that same region and AIRS CO was also historically high.

1 Satellite observation highlights of the 2010 Russian Wildfires

2
3 Jacquelyn C. Witte¹, Anne R. Douglass², Bryan N. Duncan², Arlindo M. da Silva², and
4 Omar Torres²

5
6 ¹Science Systems and Applications Inc. Lanham, MD, 20703, USA

7 ²NASA Goddard Space Flight Center, Code 613.3, Greenbelt, MD 20771, USA

8
9 Abstract

10
11 From late-July through mid-August 2010, wildfires raged in western Russia. The
12 resulting thick smoke and biomass burning products were transported over the highly
13 populated Moscow city and surrounding regions, seriously impairing visibility and
14 affecting human health. We demonstrate the uniqueness of the 2010 Russian wildfires by
15 using satellite observations from NASA's Earth Observing System (EOS) platforms.
16 Over Moscow and the region of major fire activity to the southeast, we calculate
17 unprecedented increases in the MODIS fire count record of 178 %, an order of magnitude
18 increase in the MODIS fire radiative power (308%) and OMI absorbing aerosols (255%),
19 and a 58% increase in AIRS total carbon monoxide (CO). The exceptionally high levels
20 of CO are shown to be of comparable strength to the 2006 El Niño wildfires over
21 Indonesia. Both events record CO values exceeding 30×10^{17} molec-cm².

22 23 1. Introduction

24
25 Forest fires are both a source and sink of carbon, releasing carbon dioxide (CO₂)
26 and CO to the atmosphere while burning, and removing of CO₂ during post-fire re-
27 growth, thus playing an important role in the global carbon cycle [*Olson et al.*, 1983;
28 *Crutzen and Andreae*, 1990; *Kasischke et al.*, 2005]. Russia includes approximately 30%
29 of the world's total forested area, and forest fires are common [*Alimov et al.*, 1989].
30 Despite improvements in spatio-temporal coverage of fire events due to satellite
31 monitoring, the behavior of forest ecosystems under fire conditions remains uncertain
32 [*Mottram et al.*, 2005]. Forecasting the influence of forest fires on regional and global
33 scales remains a challenge.

34 The 2010 Russian wildfires was an unprecedented forest fire event that spread
35 dangerously towards populated regions, significantly impacting human health and
36 livelihood. Media coverage was extensive and socio-economic statistics and impacts are
37 readily available in the on-line literature. A blocking high-pressure system over western
38 Russia and parts of Eastern Europe resulted in anomalously high temperatures and dry
39 conditions in July and August 2010 [*Lau and Kim*, 2010]. Our study will show that from
40 late-July through mid-August the circulation produced by the blocking event transported
41 heavy wildfire smoke and burning byproducts, such as CO, over Moscow and
42 surrounding regions. Consequently, the city experienced impaired visibility and
43 unhealthy levels of smoke and smog, compounded by local pollution sources. We use
44 observations of fire activity, smoke, and CO from several sensors on NASA's EOS
45 platforms including Aura, Aqua, and Terra to show that the 2010 Russian wildfires are
46 unique in the observing records of these sensors.

47 The next section describes the observations used in this study, followed by the
48 analyses in section 3. Included is an overview of the regional meteorological conditions
49 from daily radiosondes at various locations in the western Russia, including Moscow. We
50 also compare the 2010 Russian wildfires with the 2006 El Niño wildfires in Indonesia.

51 52 2. Satellite Data

53 54 2.1 Active Fire Counts and Fire Radiative Power

55
56 Active fire count data are taken from the Moderate Resolution Imaging
57 Spectroradiometer (MODIS) instruments on NASA's Terra and Aqua satellites that were
58 launched in December 1999 and May 2002, respectively. The Level 2 active fires
59 products MOD14 (Terra) and MYD14 (Aqua) have a pixel size of 1 km^2 at nadir
60 covering an area of $2340 \times 2030 \text{ km}$ in the across- and along-track directions, respectively.
61 The fire detection algorithm is described in *Giglio et al.*, [2003] and has been shown to
62 provide useful information about the spatial and temporal dynamics of fire activity
63 [*Giglio et al.*, 2006 and references therein]. The fire detection strategy is based on
64 absolute detection of a fire (when the fire strength is sufficient to detect), and on
65 detection relative to its background (to account for variability of the surface temperature
66 and reflection by sunlight). The Fire Radiative Power (FRP, in Megawatts) measures the
67 radiant heat output of the detected fires. *Kaufman et al.* [1996] developed an empirical
68 non-linear relationship between the MODIS mid-infrared channel brightness
69 temperatures at an active fire pixel, and the fire FRP over all wavelengths.

70 71 2.2 UV Aerosol Index

72
73 The Dutch-Finnish OMI instrument is a nadir-viewing moderate resolution
74 UV/Vis spectrometer on NASA's Aura satellite, launched on July 2004 into a sun-
75 synchronous orbit with an equator crossing-time of 13:38 in the ascending node. OMI has
76 a full cross-track swath of 2600 km, containing 60 pixels ranging from $15 \times 30 \text{ km}^2$ at
77 nadir to $42 \times 162 \text{ km}^2$ at the edge of the swath. The OMAERUV aerosol algorithm uses
78 the radiances measured at 354 and 388 nm to retrieve the UV Aerosol Index (UVAI).
79 *Torres et al.* [2007] and references therein describe the algorithm that was originally
80 developed for TOMS (Total Ozone Mapping Spectrometer). All UVAI data have been
81 filtered for the row anomalies that have affected the Level 2 data since 2007. Detailed
82 information on the OMI row anomaly can be found at
83 <http://www.knmi.nl/omi/research/product/rowanomaly-background.php>.

84 85 2.3 Total Column CO

86
87 Aqua's Atmospheric Infrared Sounder (AIRS) is a cross-track scanning grating
88 spectrometer that provides total column CO (CO_{TC}) data with a nadir 45 km field of view
89 across a 1650 km swath [*Aumann et al.*, 2003]. CO_{TC} has an estimated uncertainty for an
90 individual measurement of 7–8% with standard deviations between ± 2 and $\pm 6\%$
91 [*Yurganov et al.*, 2002]. AIRS Science Team Version 5 Level 2 daytime swaths are used
92 here.

93

94 3 Analyses

95

96 3.1 Unique Fire Event

97

98 Figure 1a shows the location of all the active fires detected by MODIS Aqua and
 99 Terra for August 2010. We observe that FRP values greater than 500 Mwatts (yellow
 100 circles) are clustered southeast of Moscow (black star). This is a region of mixed and
 101 deciduous forest with a portion consisting of peatland (USSR State Forestry Committee,
 102 1990). We focus on the southeast domain (cyan box, referred to as SE) covering 51-57°N
 103 and 37-50°E and tally the fire counts and FRP within that domain. Results are plotted in
 104 Figures 1a and 1b for June through August since 2003. We observe the following:

105 a) The fires are triggered earlier in 2010 than any previous year. On July 25th 2010,
 106 the fires ramp-up and sustain very high levels of activity and intensity through mid-
 107 August. By August 14th the fires begin to wane, while prior years show the fire products
 108 ramping up at this time and peaking later in the month.

109 b) Compared to prior years, the fires from late-July to mid-August 2010 are the
 110 most numerous and intense (two exceptions in FRP in 2008). Table 1 summarizes fire
 111 counts and FRP between July 25th and August 31st to include the 2010 fire event and
 112 seasonal fires that prior years show occurring throughout August. The statistics reveal
 113 exceptionally high values in 2010; FRP is an order of magnitude larger than previous
 114 years and the fire counts are almost doubled. The percentage increases in 2010 relative to
 115 the 2003-2009 mean are exceptionally high: 178% for fire count, and 309% for FNR.

116 At present, satellite measurements of fire activity are the best estimates of fire
 117 detection and strength [Mottram *et al.*, 2005; Roy *et al.*, 2008], however, it is important to
 118 keep the limitations of this data set in mind. In the vicinity of heavy clouds and very large
 119 fires the MODIS FRP may be less intense or not detected, resulting in a systematic low-
 120 bias in the measurements [Giglio *et al.*, 2006]. Ground fires, such as peat fires in our SE
 121 domain, generally do not produce sufficient heat to be detected by MODIS [Roy *et al.*,
 122 2008]. Only subsets of fires are captured due to the relatively large viewing geometry, i.e.
 123 pixel sizes ranging from 1 km² at nadir to 4-5 km² at edge of the swath. Thus, although
 124 MODIS captures record fires over western Russia, the actual fire detected and intensity
 125 (in FRP) may be much higher.

126

127 Table 1. Combined MODIS Aqua and Terra fire counts and FRP in the SE domain [51-
 128 57°N, 37-50°E] between July 25th and August 31st per year.

Year	Fire Count	FRP [$\times 10^4$ Mwatt]
2010	26,876	166.568
2003-2009	9683	40.729
2009	6,784	33.270
2008	18,004	94.180
2007	11,206	49.842
2006	8,582	32.320
2005	12,873	43.224
2004	8,973	28.839
2003	1,358	3.428

129

3.2 Anomalous Surface Temperatures and Relative Humidity

Lau and Kim [2010] provides a thorough analysis of the synoptic weather patterns over western Russia that set-up the ideal conditions for the wildfires to thrive, spread and intensify for a prolonged period of time. Trajectory results from the NOAA HYSPLIT trajectory model [*Draxler and Rolph*, 2010] reveal the circulation pattern produced by this blocking event. Daily clusters of backward and forward trajectories initiated during the Aqua and Terra overpass time's, for the first week in August (during the height of the fires activity: see Fig. 1) from the Moscow city center (37.6°N, 55.7°E) at levels ranging from 0.5km up to 5km show a general clockwise motion indicative of a high-pressure system (not shown). Forward trajectories from clusters of fires SE of the city show transport of air toward Moscow. Surface temperature (T_{sfc}) and relative humidity (RH_{sfc}) anomalies from 12Z daily radiosonde measurements are plotted in Figure 2 at Moscow (red) and nearby stations (locations in Fig. 2c). Data were taken from the NOAA/Earth System Research Laboratory archive (<http://www.esrl.noaa.gov/raobs/>) going back to 1994. The daily anomalies are calculated by subtracting the 1994-2009 T_{sfc} and RH_{sfc} mean from their respective 2010 values. Focusing on the summertime period accentuates the anomalously high (positive) T_{sfc} and low (negative) RH_{sfc} , relative to 2010, associated with the blocking high-pressure system. From mid-June to mid-August the range of maximum T_{sfc} and minimum RH_{sfc} at these sites is 35-41°C and 9-25%, respectively. These anomalous meteorological parameters are coincident with the maximum time period of the fires, observed in Figure 1. Wind directions from the surface up to 700 hPa from late-July to early-August 2010 are predominantly from the SE quadrant (Fig. 2d, grey shaded). This further substantiates our claim that the smoke plumes reported over Moscow during the height of the fire activity (Fig. 1) originated from wildfires largely within the SE domain.

3.3 Exceptional Smoke and CO_{TC}

The OMI UVAI is a useful parameter for tracking absorbing aerosols (i.e. smoke) even in the presence of clouds [*deGraaf et al.*, 2005] and a few recent studies have used UVAI observations to link smoke plumes to biomass burning regions [*Fromm et al.*, 2005; *Torres et al.*, 2007; *Christopher et al.*, 2008]. The UVAI 3-day running mean over the Moscow domain ($1^\circ \times 1^\circ$ area average around the city center) is plotted in Figure 3a measuring exceptionally high smoke ($\gg 1$) in early August 2010 (red). Values greater than 1 rarely occur in previous years. Coincident with the start of the fire activity (Fig. 1), UVAI builds from July 25th, returning to mean values after mid-August. Between August 5th and 10th UVAI values > 2 and large 1-sigma standard deviations $> \pm 0.4$ are observed, not seen in previous years. We do not show the UVAI within our SE domain because of significant under-sampling due to the row anomalies which, since 2009, affects almost half the OMI cross-track positions. The sparse data that are available qualitatively support the presence of elevated levels of UVAI in the SE domain.

The AIRS CO_{TC} over the Moscow and SE domains is plotted in Figure 3b. Again we see unprecedented levels of CO_{TC} peaking on August 7th of $37.1 \pm 5.1 \times 10^{17}$ molec- cm^2 in the Moscow domain (red) and $39.1 \pm 4.4 \times 10^{17}$ molec cm^2 in the SE domain (purple). We also observe elevated levels at the end of July 2006 (crosses) coincident with the

176 UVAI in Fig. 3a indicating another fire event, although short-lived compared to what we
 177 observe in 2010. Interestingly, as with the UVAI, the 1-sigma standard deviations are
 178 also large in both domains. The highest estimate occurs on August 1st at $\pm 7.4 \times 10^{17}$
 179 molec-cm² and $\pm 5.4 \times 10^{17}$ molec-cm² over the Moscow and SE domains, respectively.
 180 CO_{TC} values over both domains are comparable in magnitude to that over Sumatra and
 181 Borneo, Indonesia during the 2006 El Niño wildfires (Fig. 3b, grey dotted and dashed
 182 lines, respectively). Exceptionally high values exceeding 30×10^{17} molec-cm² are
 183 observed during both events.

184 Table 2 highlights the record high levels of CO_{TC} and UVAI in 2010 (bold)
 185 relative to prior years during the August 1-18 peak period. CO_{TC} over Moscow and SE
 186 domains increases 53% and 58%, respectively, in 2010 relative to the 2003-2009 mean.
 187 UVAI over the Moscow domain increases an order of magnitude (~255%), relative to the
 188 2005-2009 mean. Values of CO_{TC} in 2010 over both domains, including their 1-sigma
 189 standard deviations are similar to what we calculate over Sumatra and Borneo. During
 190 their peak period between October 10 and November 11, 2006 we estimate Sumatra
 191 CO_{TC} to be $34.7 \pm 3.9 \times 10^{17}$ molec-cm² and $34.9 \pm 5.3 \times 10^{17}$ molec-cm² over Borneo.

192 There is a dip in the CO_{TC} measurements over the Moscow domain on August
 193 11th and 12th, followed by a second peak in mid-August (13th-18th). The UVAI also shows
 194 a slight secondary peak (Fig. 3a). Trajectory analyses on the 11th and 12th show winds
 195 from the SE domain transporting smoke eastward, away from Moscow, while the city
 196 receives air primarily from the south and southwest where fires continue to erupt and
 197 transport smoke (Fig. 1). However, CO_{TC} remains much higher relative to previous years.

198 After August 18th CO_{TC} and UVAI return to values typical of previous years.
 199 Noteworthy is the absence of elevated CO_{TC} in the SE domain in August from 2003 to
 200 2009 concurrent with elevated active fires (Fig. 1). This may be due to the type of
 201 vegetation being burned in this region and/or that CO_{TC} is largely confined in the
 202 boundary layer where AIRS retrievals are less sensitive [Yurganov *et al.*, 2007]. Beside
 203 wildfires, peat fires may be contributing to the exceptionally high CO_{TC} in 2010. A
 204 significant portion of peat in Russia (60 Mt yr⁻¹) is used as fuel [Kolchugina and Vinson,
 205 1993]. In particular, peat fires are known to smolder for prolonged periods of time and
 206 emit large reservoirs of carbon, in the form for CO [Immirzi *et al.*, 1992; Kasischke *et al.*,
 207 2005]. The degree of involvement of peat fires during this event and the altitude of the
 208 fire plumes prior to 2010 requires further study.

209
 210 Table 2. August 1-18 mean per year of CO_{TC} [$\times 10^{17}$ molec-cm²] and UVAI [unitless] for
 211 the Moscow domain and SE domain (CO_{TC} only).

Year	SE Domain	Moscow Domain	
	[51-57°N and 37-50°E]	[1°×1° mean around the city center]	
	CO _{TC} ±1-σ	CO _{TC} ±1-σ	UVAI
2010	32.43 ± 5.05	29.47 ± 2.62	1.49 ± 0.58
2003-2009	20.48 ± 1.05	19.24 ± 0.58	2005-2009: 0.42 ± 0.19
2009	18.78 ± 0.98	17.34 ± 0.50	0.42 ± 0.13
2008	19.69 ± 1.04	17.91 ± 0.38	0.44 ± 0.23
2007	20.34 ± 1.01	18.69 ± 0.57	0.38 ± 0.18
2006	20.99 ± 1.19	19.62 ± 0.53	0.40 ± 0.23
2005	20.15 ± 0.88	18.64 ± 0.68	0.44 ± 0.20

2004	21.30 ± 1.19	20.58 ± 0.76	N/A
2003	22.09 ± 1.05	21.90 ± 0.65	N/A

212

213 4. Summary

214

215 EOS satellite multi-sensor data has enhanced our capability of tracking major
 216 atmospheric events, such as the 2010 Russian wildfires. Radiosondes stationed in western
 217 Russia measure anomalously high T_{sfc} ($> 35^{\circ}\text{C}$) and low RH_{sfc} ($< 25\%$) during the
 218 summer months. From late-July to mid-August 2010, record fires south and east of
 219 Moscow were observed by MODIS. The percentage increases in fire counts and FNR,
 220 relative to the 2003-2009 mean, are 178% and 309%, respectively. OMI UVAI over
 221 Moscow is an order of magnitude higher than previous years (255% increase). Likewise,
 222 AIRS CO_{TC} is 53% and 58% higher over the Moscow and SE domains, respectively.
 223 Exceptionally high CO_{TC} during the peak period of the Russian wildfires are comparable
 224 to what is observed during the 2006 El Niño wildfires over Sumatra and Borneo. Both
 225 events showed values exceeding 30×10^{17} molec-cm². After mid-August, MODIS fire
 226 activity drops well below what is typically seen in previous years, while UVAI and CO_{TC}
 227 return to mean values.

228

229 Acknowledgement: This work is supported by NASA's Atmospheric Chemistry,
 230 Modeling and Analysis, and Applied Sciences Air Quality Programs.

231

232 References

233

234 Alimov, Y.P., I.V. Golovikhin, L.B. Zdanevich, and I.V. Yunov (1989). Dynamics
 235 of forests under forest management organization regarding the main forest forming
 236 species in 1966-1988, *U.S.S.R State Forestry Committee*, pp. 159, Moscow.

237

238 Aumann H. H. et al. (2003), AIRS/AMSU/HSB on the Aqua Mission: Design,
 239 Science Objectives, Data Products, and Processing Systems, *IEEE Trans. Geo. Rem.
 240 Sens.*, 41, 253-264.

241

242 Christopher, S. A., P. Gupta, J. Haywood, and G. Greed (2008), Aerosol optical
 243 thicknesses over North Africa: 1. Development of a product for model validation using
 244 Ozone Monitoring Instrument, Multiangle Imaging Spectroradiometer, and Aerosol
 245 Robotic Network, *J. Geophys. Res.*, 113, D00C04, doi:10.1029/2007JD009446.

246

247 Crutzen, P. J. and M. O. Andreae (1990), Biomass Burning in the Tropics: Impact on
 248 Atmospheric Chemistry and Biogeochemical Cycles, *Science*, 250, 1669–1678.

249

250 deGraaf, M., P. Stammes, O. Torres, and R. B. A. Koelemeijer (2005), Absorbing
 251 Aerosol Index: Sensitivity analysis, application to GOME and comparison with TOMS, *J.
 252 Geophys. Res.*, 110, D01201, doi:10.1029/2004JD005178.

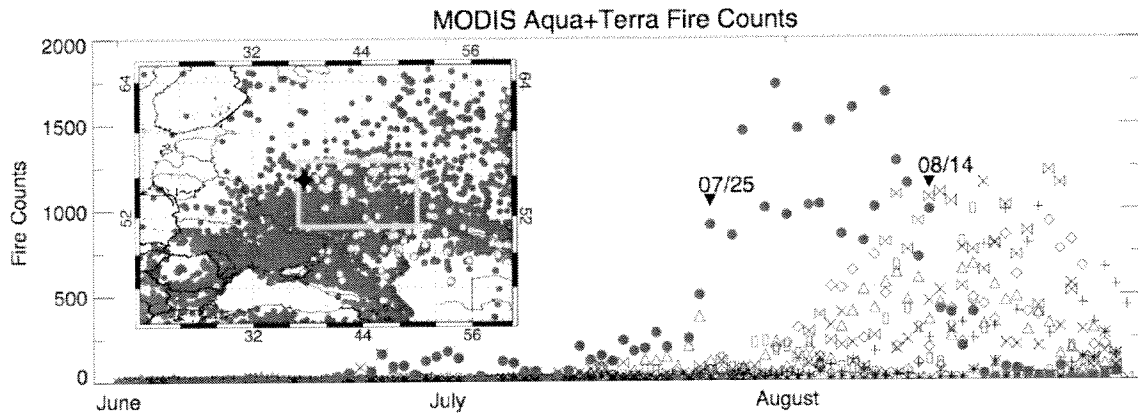
253

254 Draxler, R.R. and Rolph, G.D. (2010), HYSPLIT (HYbrid Single-Particle Lagrangian
 255 Integrated Trajectory) Model access via NOAA ARL READY Website

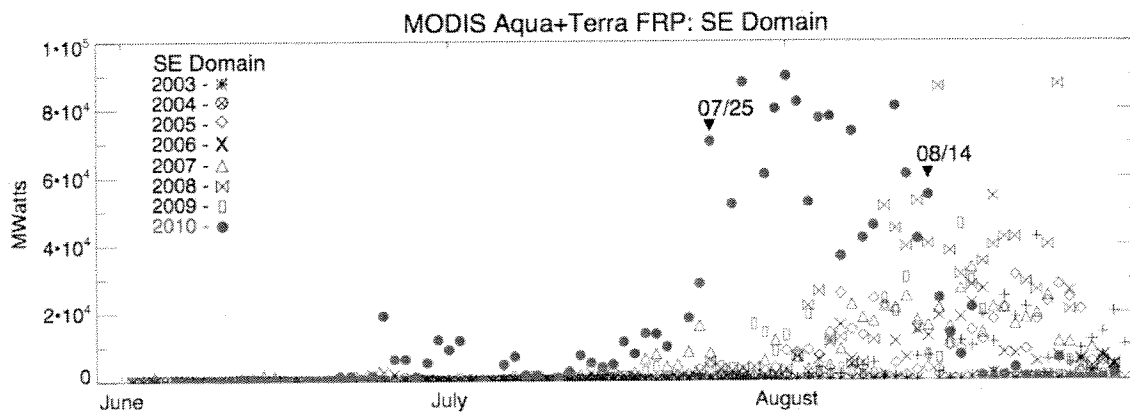
256 (<http://ready.arl.noaa.gov/HYSPLIT.php>). NOAA Air Resources Laboratory, Silver
257 Spring, MD.
258
259 Fromm, M., R. Bevilacqua, R. Servranckx, J. Rosen, J. P. Thayer, J. Herman, and D.
260 Larko (2005), Pyro-cumulonimbus injection of smoke to the stratosphere: Observations
261 and impact of a super blowup in northwestern Canada on 3–4 August 1998, *J. Geophys.*
262 *Res.*, 110, D08205, doi:10.1029/2004JD005350.
263
264 Giglio L., J. Descloitres, C. O. Justice, and Yoram J. Kaufman (2003), An enhanced
265 contextual fire detection algorithm for MODIS, *Remote Sens. Environ.*, 87, 273-282.
266
267 Giglio, L., I. Csizsar, and C. O. Justice (2006), Global distribution and seasonality of
268 active fires as observed with the Terra and Aqua Moderate Resolution Imaging
269 Spectroradiometer (MODIS) sensors, *J. Geophys. Res.*, 111, G02016,
270 doi:10.1029/2005JG000142.
271
272 Immirzi CP, E. Maltby, and R. S. Clymo (1992), The Global Status of Peatlands and
273 Their Role in Carbon Cycling. London: Wetlands Research Group, Friends of the Earth;
274 1992. Rep. No. 11.
275
276 Kasischke, E. S., E. J. Hyer, P. C. Novelli, L. P. Bruhwiler, N. H. F. French, A. I.
277 Sukhinin, J. H. Hewson, and B. J. Stocks (2005), Influences of boreal fire emissions on
278 Northern Hemisphere atmospheric carbon and carbon monoxide, *Global Biogeochem.*
279 *Cycles*, 19, GB1012, doi:10.1029/2004GB002300.
280
281 Kolchugina, T.P. and T.S. Vinson (1993), Comparison of two methods to assess the
282 carbon budget of forest biomes in the Former Soviet Union, *Water, Air, And Soil*
283 *Pollution*, 70, 207-221.
284
285 Kaufman, Y., L. Remer, R. Ottmar, D. Ward, L. Rong-R, R. Kleidman, R. Fraser, L.
286 Flynn, D. McDougal, and G. Shelton (1996), Relationship between remotely sensed fire
287 intensity and rate of emission of smoke: SCAR-C experiment, in *Global Biomass*
288 *Burning*, edited by J. Levine, pp. 685 – 696, MIT Press, Cambridge, Mass.
289
290 Lau W. K. M. and K. M. Kim, The 2010 Pakistan Flood and the Russia Heat Wave:
291 Teleconnection of Extremes, *Nature Geosciences*, submitted, 2010.
292
293 Mottram G. N., M. J. Wooster, H. Balster, C. George, F. Gerrard, J. Beisley (2005), The
294 use of MODIS-derived fire radiative power to characterise Siberian boreal forest fires,
295 *Proceedings of the 31st international symposium on remote sensing of environment*, St.
296 Petersburg, Russian Federation, 20–24 June 2005.
297
298 Olson, J. S., J. A. Watts, and L. J. Allison (1983). Carbon in live vegetation of major
299 world ecosystem, ORNL-5862, Oak Ridge.
300

301 Roy, D.P., L. Boschetti, C. O. Justice, and J. Ju (2008), The Collection 5 MODIS Burned
302 Area Product - Global Evaluation by Comparison with the MODIS Active Fire Product,
303 *Remote Sens. Environ.*, 112, 3690-3707.
304
305 Torres, O., A. Tanskanen, B. Veihelmann, C. Ahn, R. Braak, P. K. Bhartia, P. Veeffkind,
306 and P. Levelt (2007), Aerosols and surface UV products from Ozone Monitoring
307 Instrument observations: An overview, *J. Geophys. Res.*, 112, D24S47,
308 doi:10.1029/2007JD008809.
309
310 USSR State Forestry Committee (1990), *Forest Fund of the USSR*, Vol 1, 1005 pp.,
311 Moscow.
312
313 Yurganov, L. N., W. W. McMillan, A. V. Dzhola, E. I. Grechko, N. B. Jones, and G. R.
314 van der Werf (2008), Global AIRS and MOPITT CO measurements: Validation,
315 comparison, and links to biomass burning variations and carbon cycle, *J. Geophys. Res.*,
316 113, D09301, doi:10.1029/2007JD009229.

317 Figure 1. Combined Aqua and Terra fire counts and FNR over the SE domain are plotted
 318 in (a) and (b), respectively. Map inset in (a) of Aqua and Terra fire counts (red circles).
 319 Yellow circles indicate FNR > 500 Mwatts. Star marks the location of Moscow. The cyan
 320 box defines the SE domain covering 51-57°N and 37-50°E.

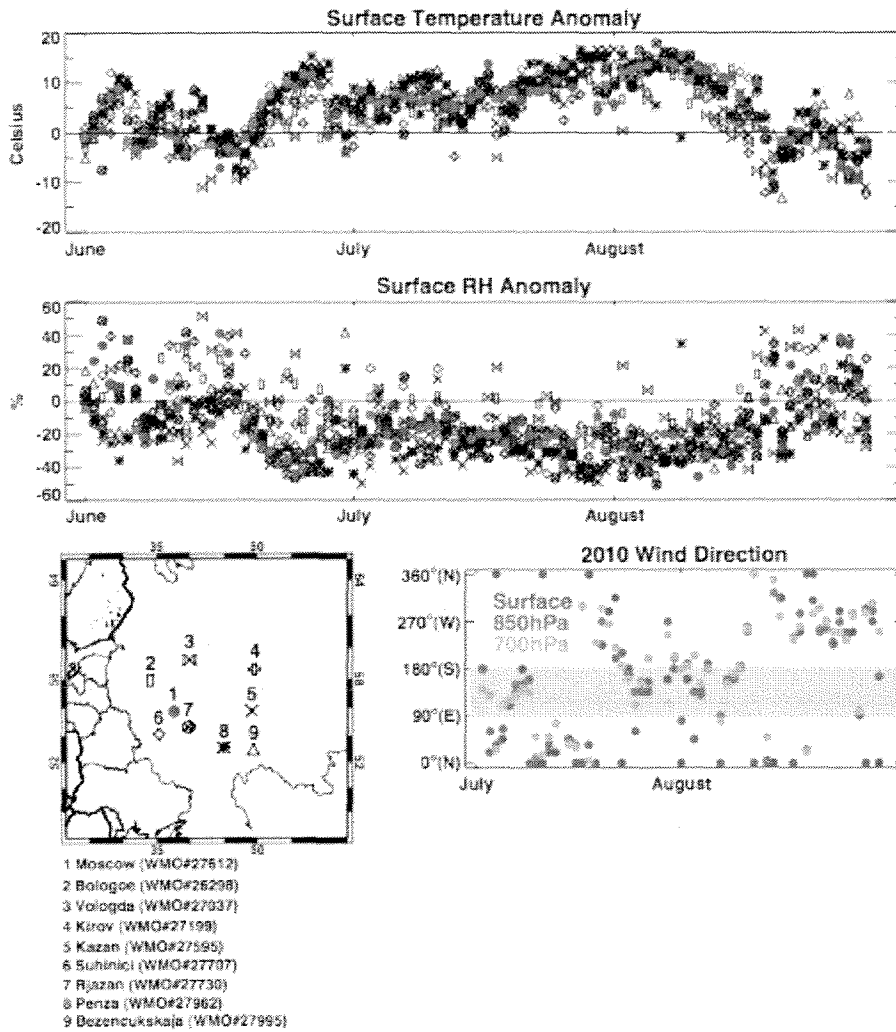


321



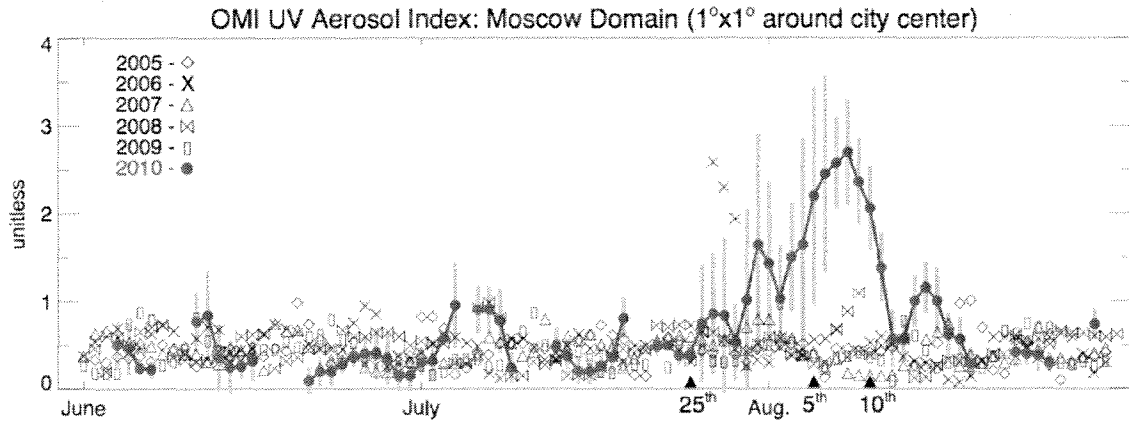
322

323 Figure 2. (a) T_{sfc} and (b) RH_{sfc} anomalies. Radiosonde locations, including symbol legend
 324 for (a) and (b) are mapped in (c). Wind directions in July and August 2010 are shown in
 325 (d) at the surface (red), 850hPa (blue), and 700hPa (green). Grey shading highlights the
 326 southeast quadrant.

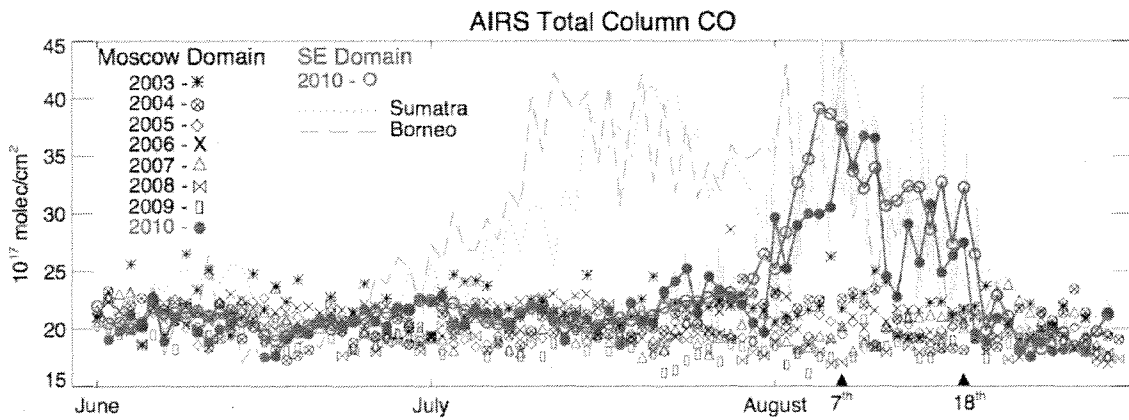


327
 328

328 Figure 3. (a) UVAI plotted per year over the Moscow domain between June and August.
 329 2010 is highlighted in red. CO_{TC} in (b) plotted similar to (a), also including the SE
 330 domain (purple). The 1- σ standard deviations are plotted for 2010 only in grey shading.
 331 Sumatra [96-107°E, 7°S-5°N] (grey dotted) and Borneo [109-119°E, 5°S-5°N] (grey
 332 dashed) are overlaid in (b) for September - November 2006.



333



334